JOURNAL OF APPLIED ELECTROCHEMISTRY 12 (1982) 505–515

Galvanostatic cycling of graphite intercalation electrodes with anions in aqueous acids

F. BECK, H. KROHN, W. KAISER

University of Duisburg Gesamthochschule FB 6 Elektrochemie, D 4100 Duisburg 1, Lotharstraße 63, FR Germany

Received 12 December 1981

Natural graphite flakes (80 wt%), with polypropylene (20 wt%) as a binder, constitute a practical and non-expensive graphite electrode of high crystallinity 'CPP'. Galvanostatic cycling of these electrodes with current densities in the range 0.3–30 mA cm^{-2} (charging time 5–120 min) has been investigated in aqueous acids (12, 20 and 36 mol dm^{-3} HF, 6 and 12 mol dm^{-3} H_2SO_4, 4 mol dm^{-3} $HClO_4$). The anion of the acid is anodically intercalated and cathodically de-intercalated. In spite of the high water concentrations, quantitative current efficiencies have been obtained. From variation of the rest times after charging, a corrosion current density of less than 0.03 mA cm^{-2} (j_{ch} = 3 mA cm^{-2}) has been derived. The overvoltage during charge and discharge is typically about 0.1 V. The potential at the start of the charging process coincides with the intercalation potential defined previously. A strong electrode formation effect is observed upon cycling. The electrode is initially smooth and non-porous; it acquires a high surface roughness after a few cycles, which is then stable. The initial charging curves increase with $t^{1/2}$, while the charging curve after electrode formation is linear. Both clearly indicate a linear relationship between surface concentration of intercalated anions and potential. This agrees with our previous finding of linear dependence with respect to acid concentration in the solution.

1. Introduction

Carbon and graphite are non-expensive electrode materials, which are readily available. Generally they behave as inert electrodes with no change in the bulk of the solid phase. However, since the work of Rüdorff and Hofmann [1, 2], it is well known, that crystalline graphite can be anodically converted to graphite salts, where anions are intercalated between the carbon planes. The de-intercalation proceeds via corrosion or cathodic polarization. The crystals of natural graphite used at that time or the pyrolytic graphite investigated later [3] were not very practical electrodes to use due to a total disintegration into lamella after a few cycles. Moreover, concentrated acids, which were regarded as necessary to overcome 'hydrolysis', suffered from several drawbacks, not least that of reduction at the negative electrode and low conductivity.

We have reported previous systematic work with natural graphite composite electrodes with a polypropylene binder, 'CPP', originating from the development of a dissolved lead secondary battery [4, 5]. This kind of nonporous crystalline graphite electrode proved to be very stable upon cycling. We have obtained up to 3000 cycles (3 mA cm^{-2}, 1 h charge) with it. Moreover, we have found that high current efficiencies can be obtained even in non-concentrated acids, containing 50–80% H_2O [6, 7]. Secondary cells with smooth electrodes of Cu, Pb, Fe and Zn are under investigation [8]. 20–60% HF proved to be a very interesting electrolyte [9]. Reversible cycling of these electrodes is even possible in neutral salt solutions [10].

We wish to report further results which were obtained with single electrodes under galvanostatic conditions. The parameters are adjusted for a potential application in secondary batteries [8] and for transport limitation in the solid phase, which is generally to be expected. This means that the galvanostatic experiments were done in a cyclic mode, and that the standard current density was 3 mA cm^{-2}. Also for practical reasons, most

0021-891X/82/050505-11$03.82/0

of the experiments were carried out in H_2SO_4 and HF, which are very economical electrolytes.

2. Experimental procedure

The electrolytes were prepared with distilled water and 40 and 73% HF 'reinst', from Fluka and 97% H_2SO_4 p.a. and 72% $HClO_4$ p.a. from Merck. The concentrations were 4 mol dm^{-3} $HClO_4$, 6 and 12 mol dm^{-3} H_2SO_4, and 12, 20, 36 and 50 mol dm^{-3} HF (22, 5, 36, 60 and 80 wt% HF).

The graphite *electrode material* which was used in this work was composed of 80 wt% natural graphite flakes (Kropfmühl, Munich) and 20 wt% polypropylene as a binder. The natural graphite 'Normalflocke' was specified to contain 94 wt% graphite and 6 wt% ash*, which itself is composed of 45% SiO_2, 26% Al_2O_3, 11% insoluble Fe_2O_3, 11% soluble Fe_2O_3, 5% CaO and 2% MgO. Plates 0.3 cm thick were manufactured from this mixture in a hot press (190° C, 10 bar) [11]. The material has a resistivity of about 1 Ω cm and is called 'CPP'. The density is 1.7 g cm^{-3}. Before using the electrode, a thin polymer film is removed from the surface by scraping with a glass edge or by sand-blasting, cf. [7].

The *electrode design* is represented schematically in Fig. 1. Pieces of CPP-plates, 55 mm × 20 mm × 3 mm, were covered with a special, self-adhering plastic (PVC) sheet. A 'window' of 10 mm × 10 mm was cut into it to yield the electrode area. In this region the polymer film on the material was removed by scraping. The electrode was contacted at the upper end with a brass sup-

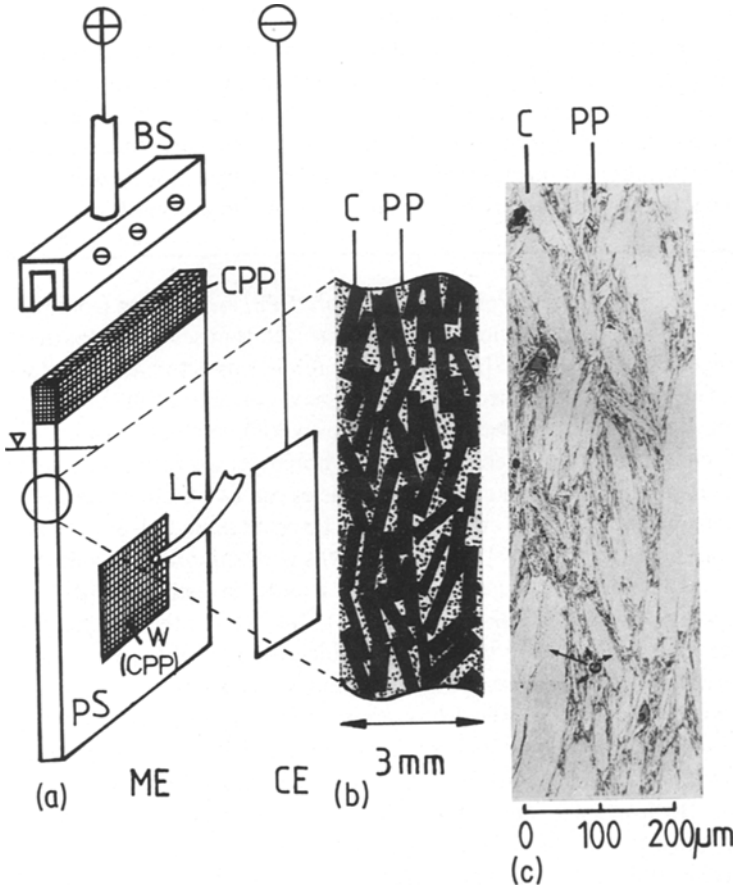

Fig. 1. (a) Design of measuring electrode ME. CE = counter electrode, LC = Luggin capillary, PS = plastic sheet, BS = brass support, W = window. (b) Schematic composition of CPP. (c) SEM micrograph of CPP-material, polished along the thickness of the plate.

* Experiments with CPP, filled with 99.95% natural graphite flakes, showed clearly that the ash content did not influence the intercalation process.

port. Fig. 1 shows clearly that the graphite flakes are oriented approximately, but not exactly parallel to the surface, thus opening a lot of ridges after scraping which are useful in the intercalation process.

The *cell* was made of polyethylene. A counter-electrode of CPP and a reference electrode Hg/Hg_2SO_4 in 1 mol dm^{-3} H_2SO_4 ($E = +674$ mV vs SHE) was placed in the cell. The potentials measured versus this electrode are called E_s in this paper. The temperature was 20° C. The electrolyte was stirred magnetically and its conversion was well below 0.1% during one cycle. The current density was controlled by an AMEL bigalvanostat, Model 545, in combination with two Indigel datatimers (10^{-2}–10^5 s) by selecting charging and resting times. The charging times were in the range of 0.5–120 min. With a standard current density of 3 mA cm^{-2}, this leads to a conversion of CPP (in reference to an upper limit of $C_{24}^{+}A^{-}$) of up to 16%, or 32%, if both sides are charged. The charge density reaches 0.6 Ahdm^{-2}. The discharge was continued, until a final potential of $E_s = 0$ V was reached; then, the next cycle was started. The term 'current efficiency', α, used in this work is defined as a round-trip current efficiency (c.e.)

$$\text{c.e.} = \frac{\text{discharge capacity, } Q_{dis}}{\text{charge capacity, } Q_{ch}}. \qquad (1)$$

3. Results

3.1. *General behaviour upon cycling*

Some typical examples of charge/discharge curves with rest periods between are shown in Figs. 2 and 3. The charge process starts at very positive potentials, with increases of up to 0.3 V, depending on the cycle number, Z, and length of the charging period. In the rest period after charge, t_0, the potential decays rapidly initially, but attains a stable value after about 30 min. The discharge curve generally observed is S-type. In more dilute acids (4 mol dm^{-3} $HClO_4$) and after an extended charge process at higher potentials (for long charge times or high current densities), this type of discharge curve is appreciably distorted. The difference between the average charge and discharge voltage is relatively small. It is characteristic of this unusual type of battery electrode, which is primarily smooth and nonporous, that the first cycle and to some minor extent the second cycle differ clearly from later cycles, after the establishment of a steady-state. Thus a rapid and very effective formation process occurs upon cycling. The current efficiency increases appreciably, and the charging curves become linear in all cases.

3.2. *Formation of CPP upon cycling*

The linearization of the charging curves is again demonstrated in Fig. 4. A sequence of experiments with increasing charge time is compiled in this figure. While the first charging curves almost coincide, the situation in the seventh cycle has changed completely. The curves have attained linearity, and the slope flattens with increasing charge time, which is due to a more extended formation in this case.

The current efficiency increases in the course of the first 3–6 cycles and reaches a steady-state thereafter. This is shown in Fig. 5 for three electrolytes. The formation process is somewhat dependent on the length of the rest time; in some cases, e.g. 20 mol dm^{-3} HF at 0.5 h charge, the current efficiency decreases again at higher cycle numbers.

3.3. *Variation of rest time–corrosion behaviour*

The rest time t_0 was systematically varied in order to investigate the corrosion of the graphite intercalates under practical conditions. A plot of α versus t_0 generally yielded straight lines. The intercept on the α-coordinate leads to the corrected current efficiency, α_0, (neglecting the corrosion in the course of discharge). From the slope of the curve, the corrosion current density, j_{corr}, can be calculated according to

$$j_{corr} = \frac{\Delta\alpha}{\Delta t_0} Q_{ch}. \qquad (2)$$

In Fig. 6, the above plots are shown for various acids at half-hour charge rates. All measurements of this kind have been evaluated using Equation 2; the results are collected in Table 1. The j_{corr} values are in some cases below 1% of j_{ch}, the charging current density, indicating a rather low rate of corrosion even in the presence of elevated water concentrations. The corrected current efficiencies,

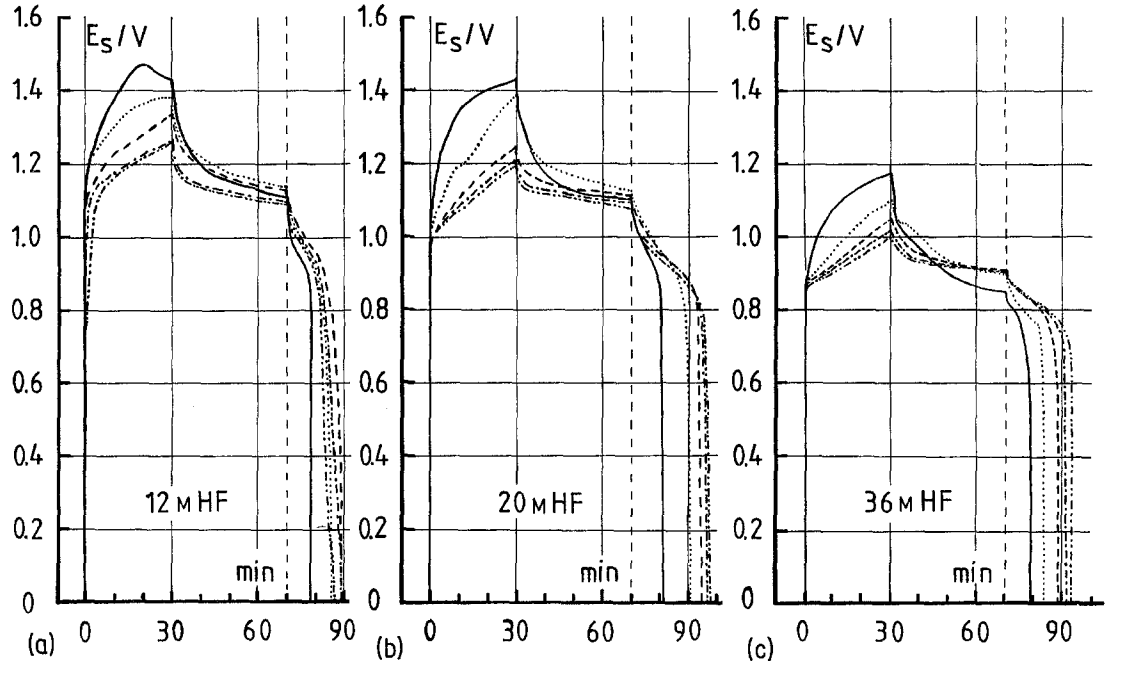

Fig. 2. Charge/discharge curves of CPP with 3 mA cm^{-2}, t_{ch} = 0.5 h, rest time, t_0 = 40 min and deep discharge to E_s = 0 V. Electrolytes: A = 12 mol dm^{-3}, B = 20 mol dm^{-3} and C = 36 mol dm^{-3} HF. —— 1st cycle, · · · · · 2nd cycle, - - - - - 4th cycle, - · - · - 7th cycle, - · - · - · - 9th cycle.

α_0, show quantitative behaviour in some examples. A further discussion of Table 1 is given in Section 4.5.

An example of the influence of *charge times* on the charging curve has already been given in Fig. 4. In Fig. 7, it is shown, how α decreases with increasing charge time. This effect is mainly due to penetration of the charging curve into the potential region where excessive side reactions occur at the surface of the electrode. The charging potential limit seems to be between ΔE_{ch} = 0.2 and 0.25 V, in agreement with our findings with the slow cyclovoltammetric method [7]. At very low charge densities, the curve drops again due to competition with the recharging of surface groups.

The influence of the *electrolyte* and its concentration on the current efficiency is in good agreement with our former results, which were obtained using slow cyclic voltammetry [6, 7]. In the HF-systems, high current efficiencies can be realized

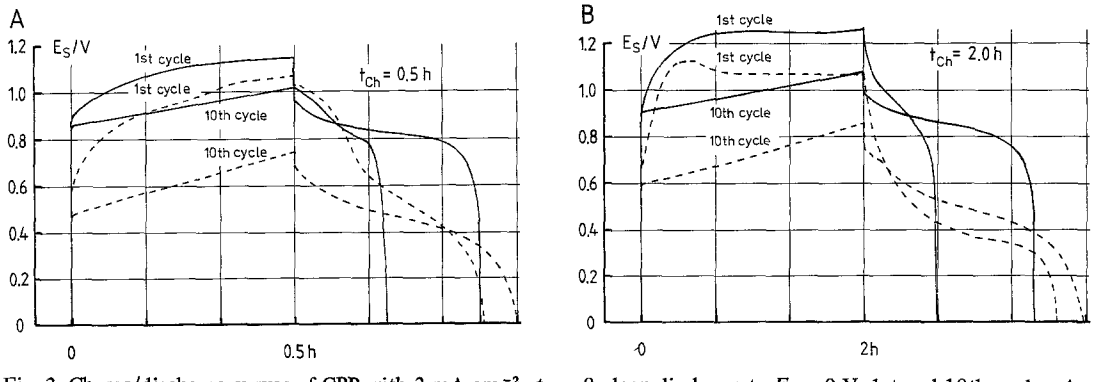

Fig. 3. Charge/discharge curves of CPP with 3 mA cm^{-2}, t_0 = 0, deep discharge to E_s = 0 V. 1st and 10th cycles. A, t_{ch} = 0.5 h and B, t_{ch} = 2.0 h. —— 36 mol dm^{-3} HF and - - - - - 12 mol dm^{-3} H_2SO_4.

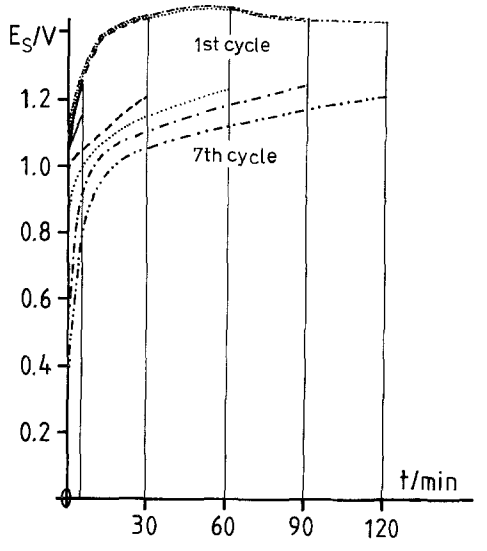

Fig. 4. Charging curves in 20 mol dm^{-3} HF, 1st and 7th cycles, 3 mA cm^{-2}. —— t_{ch} = 5 min, - - - - - t_{ch} = 30 min, · · · · · t_{ch} = 60 min, - · - · - t_{ch} = 90 min, - · · - · · - t_{ch} = 120 min.

in a medium concentration range of 40–70 wt% HF. This is of special interest for practical applications due to the very positive potentials under these conditions. In nearly anhydrous HF, the current efficiency drops below 50%, and the discharge curve degenerates. This also agrees with our findings with slow cyclovoltammetry [9]. Medium water concentrations seem to be an essential factor in the reversible cyclic behaviour of the HF-system.

3.4. *Variation of the current density*

The current densities of charge and discharge of the CPP-electrode have been systematically varied in the range 0.3 to 30 mA cm^{-2}. The corresponding curves in 20 mol dm^{-3} HF are shown in Fig. 8 for the 10th cycle. The discharge curve for the high charge rate experiment (curve 1) shows a section at lower potentials. Further discharge at lower current densities results in the recovery of only small additional discharge capacities. The variation of current efficiency with current density is shown in Fig. 9 for three electrolye solutions. Normally, α decreases at higher current densities as a result of enhanced side reactions mainly in the course of the charging process. At low discharge current densities, α decreases as well, which is caused by the accompanying corrosion reaction.

3.5. *Mixtures of H_2SO_4 and HF*

Mixtures of H_2SO_4 and HF play some role in cells with metal electrodes, which behave better in such systems compared with systems using single acids. The intercalation potential differs greatly in the two acids, depending on their concentration, cf. Table 2. Fig. 10 shows that the average charge and discharge potentials increase linearly with increasing volume concentration of 20 mol dm^{-3} HF. On the other hand, α decreases from nearly 100% in

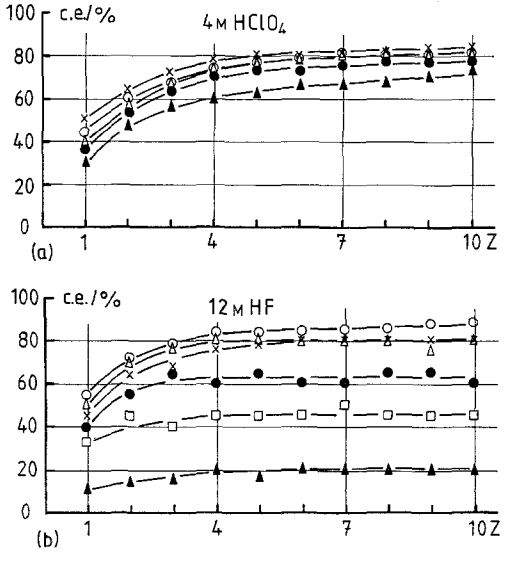

Fig. 5. Development of α with Z due to electrode formation. a, 4 mol dm^{-3} $HClO_4$, t_{ch} = 30 min. b, 12 mol dm^{-3} HF, t_{ch} = 5 min. c, 20 mol dm^{-3} HF, t_{ch} = 30 min. Resting times: X——X t_0 = 0 min. ○——○ t_0 = 15 min. △——△ t_0 = 40 min. ●——● t_0 = 100 min. □——□ t_0 = 180 min. ▲——▲ t_0 = 250 min.

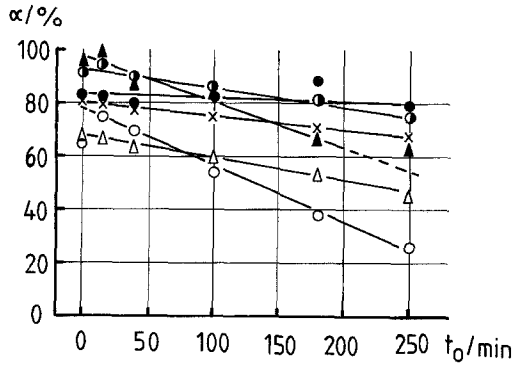

Fig. 6. Plot of current efficiency, α, versus rest time, t_0, for various acids, $t_{ch} = 0.5$ h. Average cycles, 5 to 10. ×——× 4 mol dm^{-3} $HClO_4$, ▲——▲ 6 mol dm^{-3} H_2SO_4, △——△ 12 mol dm^{-3} H_2SO_4 (average cycles = 4–6), ○——○ 12 mol dm^{-3} HF, ○——○ 20 mol dm^{-3} HF, ●——● 36 mol dm^{-3} HF (average cycles = 9, 10).

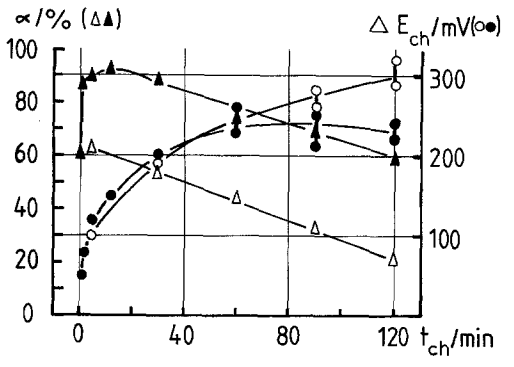

Fig. 7. Plot of current efficiency, α, and ΔE_{ch} versus charging time t_{ch}. Average of α taken between the 5th and 10th cycles. ○, ● ΔE_{ch} (mV); △, ▲ α; ●, ▲ 20 mol dm^{-3} HF; ○, △ 12 mol dm^{-3}.

mixtures rich in 12 mol dm^{-3} H_2SO_4 to only 60% in 20 mol dm^{-3} HF. These experiments have been performed with two hourly charging rates.

3.6. *Intercalation potential*

We have defined the potential at which a steep current rise is observed in the slow cyclovoltammetric method due to anodic intercalation as the intercalation potential, E_I, [7]. Surprisingly, we have found that the effect depends *linearly*, not logarithmically, on the acid concentration [7, 9]. In this work, the potentials at the beginning of galvanostatic charging are in good agreement with the intercalation potentials, as shown in Table 2.

4. Discussion

4.1. *Competition between graphite salt/graphite oxide formation and decomposition*

Current efficiency, α, defined in Equation 1 is the product of the material current efficiency, λ, during the charge process

Table 1. Evaluation of corrosion current density of CPP in various electrolytes and dependence of charge density

Electrolyte	Q_{ch} (mA min cm^{-2})	j_{corr} (mA cm^{-2})	α_0 (%) ($t_0 = 0$)
4 mol dm^{-3} $HClO_4$	15	0.027	95
4 mol dm^{-3} $HClO_4$	90	0.050	81
6 mol dm^{-3} H_2SO_4	90	0.075	71
12 mol dm^{-3} H_2SO_4	15	0.020	98
12 mol dm^{-3} H_2SO_4	90	0.17	99
12 mol dm^{-3} H_2SO_4	360	0.16	95
12 mol dm^{-3} HF (≈ 22 wt%)	15	0.04	(80)
12 mol dm^{-3} HF (≈ 22 wt%)	90	0.20	65
12 mol dm^{-3} HF (≈ 22 wt%)	360	0.36	34
20 mol dm^{-3} HF (38 wt%)	15	0.013	100
20 mol dm^{-3} HF (38 wt%)	90	0.068	94
20 mol dm^{-3} HF (38 wt%)	360	0.20	82
36 mol dm^{-3} HF (60 wt%)	90	≈ 0.01	85
36 mol dm^{-3} HF (60 wt%)	360	≈ 0.02	76
48 mol dm^{-3} HF (80 wt%)	90	≈ 0.01	95
48 mol dm^{-3} HF (80 wt%)	360	–	91
48 mol dm^{-3} HF (100 wt%)	90	–	45

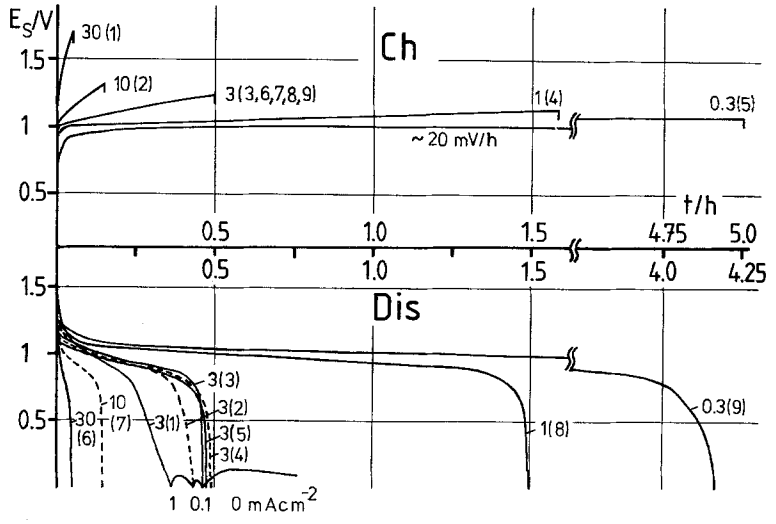

Fig. 8. Charge/discharge curves with CPP at various current densities, indicated at the curves (in mA cm^{-2}), in 20 mol dm^{-3} HF, 10th cycle, $t_0 = 0$, $Q_{ch} = 90$ mA min cm^{-2} = constant. Numbers in brackets indicate j_{ch}/j_{disch} in mA cm^{-2}. (1) 30/3, (2) 10/3, (3) 3/3 (standard), (4) 1/3, (5) 0.3/3, (6) 3/30, (7) 3/10, (8) 3/1, (9) 3/0.3.

$$n = \lambda \frac{Q_{ch}}{zF} \tag{3}$$

and of the electrical current efficiency, ϵ, during the discharge process [12]

$$Q_{dis} = \epsilon z F n. \tag{4}$$

where n is the number of moles, z is the charge and F is Faraday's constant. Thus from these two equations:

$$\alpha = \lambda\epsilon = \frac{Q_{dis}}{Q_{ch}}. \tag{5}$$

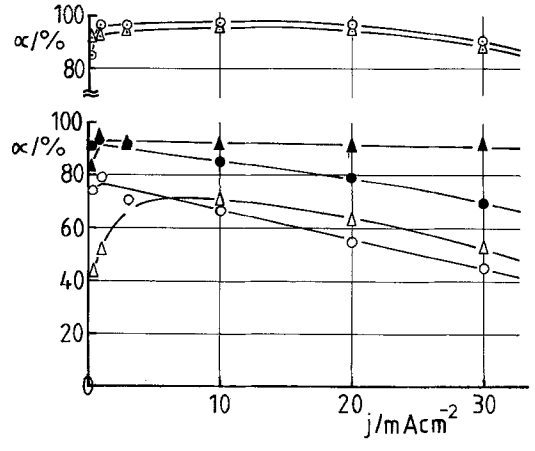

Fig. 9. Plot of current efficiency, α, versus current density j, $Q_{ch} = 90$ mA min cm^{-2}. Average values of α taken between the 5th and 10th cycles. ○ ● ⊙ variable j_{ch}, $j_{dis} = 3$ mA cm^{-2}. △ ▲ ⧋ variable j_{dis}, $j_{ch} = 3$ mA cm^{-2}. ○ △ 12 mol dm^{-3} HF. ● ▲ 20 mol dm^{-3} HF. ⊙ ⧋ 12 mol dm^{-3} H_2SO_4.

A secondary cell is not in equilibrium, if the α values differ at both electrodes. A deficiency in α, which is normally observed, can be explained as a nonquantitative λ and/or ϵ. If λ *is not quantitative*, the graphite salt is not generated ideally. In our case, this is mainly due to competing formation of graphite oxide, which is formed via the graphite salt [13]. When the graphite salt has finally accumulated as $C_{24}A$ at the surface, part of it diffuses further into the bulk of the electrode, but another part reacts to give graphite oxide according to:

$$C_{24}A + H_2O \rightarrow C_{24}OH + H^+ + A^-(aq). \tag{6}$$

This means, that the charging current is split into two portions, that for diffusion (diff) and that for graphite oxide (g.o.):

$$j = j_{diff} + j_{g.o.}. \tag{7}$$

The mobility of the graphite oxide is much lower. Its formation may be limited by water transport. The reduction of graphite oxide is retarded due to high transport overvoltages, see example (1) in Fig. 8 and the work of Besenhard and Fritz [14].

Nonquantitative ϵ values are due to diffusion resistance during discharge. At the end of discharge, the surface concentration on the electrode may be totally depleted, cf. Section 4.6.

4.2. *Interpretation of the formation effect*

Our experiments start with a smooth, nonporous CPP-electrode. In the course of the first cycle, the

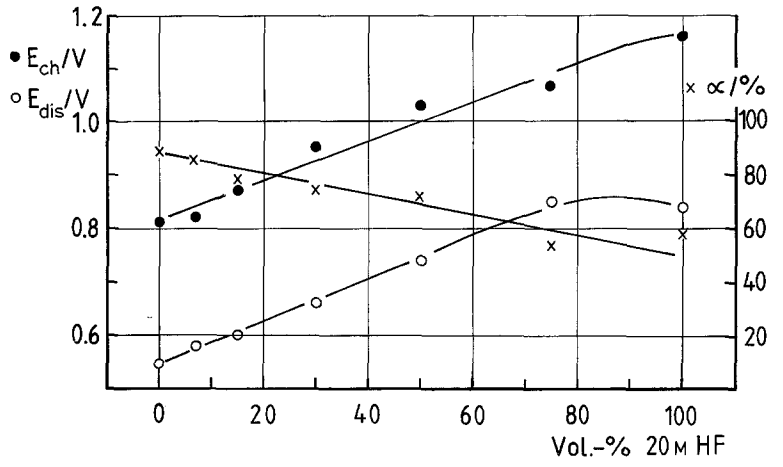

Fig. 10. Behaviour of H_2SO_4/HF mixtures. Vol% means volume ratio of 12 mol dm^{-3} H_2SO_4 and 20 mol dm^{-3} HF *before* mixing of the acids. •——• increase of average E_{ch} with increasing HF concentration. ○——○ increase of average E_{dis} with increasing HF concentration. ×——× decrease of current efficiency, α, with increasing HF concentration (average of 5–10 cycles).

graphite flakes near the surface swell during charge and shrink again during discharge. This volumetric cycle leads directly to a porous structure for the intercalation electrode. The surface roughness of the electrode obviously increases. A further formation effect is established in the course of the subsequent cycles. However, this does not lead to a mechanical disintegration of the electrode due to an ideal and stable binder. No shedding of the graphite flakes is observed even after 3000 cycles [8].

4.3. *Transport in the solid phase and analysis of the charging curve*

According to this mechanism, the type of transport of the intercalated anion changed fundamentally after a few cycles. Initially, a half infinite diffusion into the bulk of the nonporous plate must be anticipated. The time constant, τ, for this diffusion process,

$$\tau = \frac{d^2}{D}, \tag{8}$$

is large, with D, the diffusion coefficient, equal to 10^{-8} cm^2 s^{-1} [6, 7] it is in the order of 10^7 s. d is the electrode thickness. Thus, the opposite boundary of the plate electrode does not play any role in the course of the experiment. Upon charging, the surface concentration, c_0, of the intercalated anion increases with time according to a square root function (Sand equation):

$$c_0 = \frac{2j}{zF(\pi D)^{1/2}} t^{1/2} \tag{9}$$

The concentration profiles in the electrode develop according to Fig. 11a.

If we assume a *linear* dependency of the intercalation potential on the surface concentration, we obtain

$$\Delta E_I = E_I - E_{I,0} = K c_0 \tag{10}$$

Table 2. A comparison of intercalation potentials E_I *after* [7] *and* [9] *with the potentials at the beginning of the charging curves*

Acid	$E_{I,s}$(V) *Cyclic voltammetry*	$E_{I,s}$(V) *Galvanostatic charging*
4 mol dm^{-3} $HClO_4$	0.95	0.93
6 mol dm^{-3} H_2SO_4	0.98	0.94
12 mol dm^{-3} H_2SO_4	0.63	0.60
12 mol dm^{-3} HF	1.12	1.12
20 mol dm^{-3} HF	1.01	1.00
36 mol dm^{-3} HF	0.81	0.88
48 mol dm^{-3} HF (80%)	0.78	0.76
48 mol dm^{-3} HF (≈ 100%)	0.73	0.68

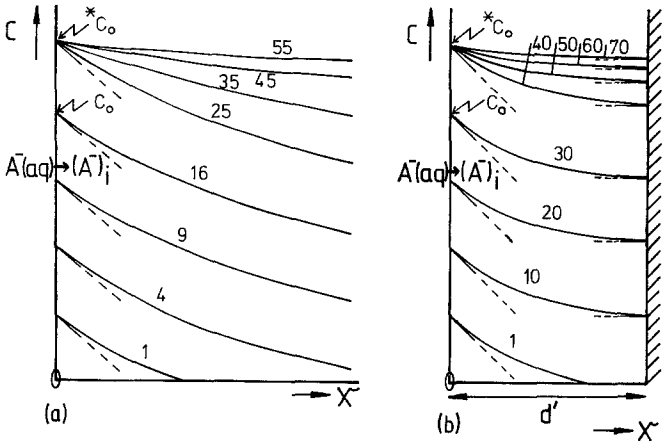

Fig. 11. Schematical representation of concentration profiles. Numbers indicate relative times. (a) Semi-infinite diffusion. (b) Limited diffusion (thickness of plane plate = d').

where $E_{I,0}$ is the intercalation potential at the very beginning of the intercalation process and K is a constant. The potential increases smoothly rather than in steps, which should be expected due to the 'stages' $C_{96}A$, $C_{72}A$, $C_{48}A$ and $C_{24}A$ [3]. This can be rationalized in terms of random charging of the graphite flakes. According to our general experience, ΔE_I is equal to 0.25 V for $C_{24}A$, which is the maximum possible surface concentration. This corresponds to an anion concentration of 5.7 mol dm^{-3} in the solid, if we assume a density of 1.5. From this, K can be calculated as 44 V cm^3 mol^{-1}.

In Fig. 12, some primary charging curves are evaluated in terms of the last two equations.* The square root function is essentially realized. From the slope of the curves, a diffusion coefficient can be calculated to be $D = 3.2 \times 10^{-8}$ cm^2 sec^{-1} for HSO_4^- and $D = 1.5 \times 10^{-7}$ cm^2 sec^{-1} for HF_2^-. The former value is in good agreement with the results of three other, independent methods with ClO_4^- anions [6, 7]. The diffusion coefficient of HF_2^- is appreciably larger, cf. [9]. It must be stressed that the diffusion coefficient gained in this way is an average property of the CPP-plate rather than a property of an individual graphite flake. However, the latter can be calculated from this if the angle between the flakes and the geometric plane is known, together with the mean diffusion length in a flake.

* Due to the slightly inclined orientation of the graphite flakes with reference to the electrode surface, the geometric current density differs widely from that in the a-direction.

After a few cycles, formation of the electrode leads to the charge of the single flakes in the electrode. The time constant drops dramatically due to the smaller dimension of the particle. From Fig. 1 the mean a-dimension of the graphite flakes is about 0.2 mm. Thus, the mean diffusion length d' from the edge of the flake to the centre is about 0.1 mm. However, this length is reduced further due to imperfections in the crystal. Thus the transport mechanism changes to a finite diffusion problem, a 'filling-up' of the total crystal. The corresponding profiles are shown in Fig. 11b. The mathematical problem has been treated for heat transfer [15], cycling of an amalgam film [16] and cycling of a TiS_2 intercalation electrode [17]. Neglecting the early stages of the process, the steady-state expression for the surface concentration becomes very simple:

$$c_0 = \frac{j_{ch}}{Fd'} t. \tag{11}$$

Together with Equation 10, a linear charging curve must be expected in the later cycles, which is actually the case. The slope of the curves seem to depend only on the real current density, this means on the roughness factor, f, of the electrode formed. For a charging time, $t_{ch} = 0.5$ h and number of cycles, $Z = 5$, the linear curve increases in all electrolytes by 0.25 V (range of reversible intercalation up to $C_{24}A \equiv 5.7$ mol dm^{-3} as c_0) within 30–35 min. With this slope and assuming a roughness factor of 10 ($j_{true} = 0.3$ mA cm^2), a thickness of $d' = 10^{-3}$ cm can be calculated from the

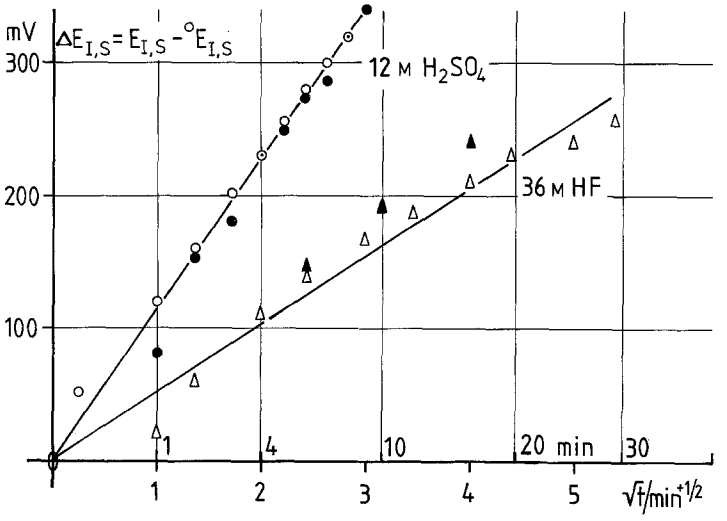

Fig. 12. Plot of the increase of intercalation potential $\Delta E_{I,S}$ versus the square root of the time for the first cycle. ○ ● 12 mol dm^{-3} H_2SO_4, △ ▲ 36 mol dm^{-3} HF.

last two equations. The time constant drops to 200 s.

Our results on graphite bed electrodes confirm these findings. The charging curve is strongly linear from the beginning of the cycling experiment. Every flake is charged individually.

From Fig. 8, a constant product of j_{ch} and rise time of linear potential increase can be derived, if ΔE_I remains below 200 mV. This is further support for our model.

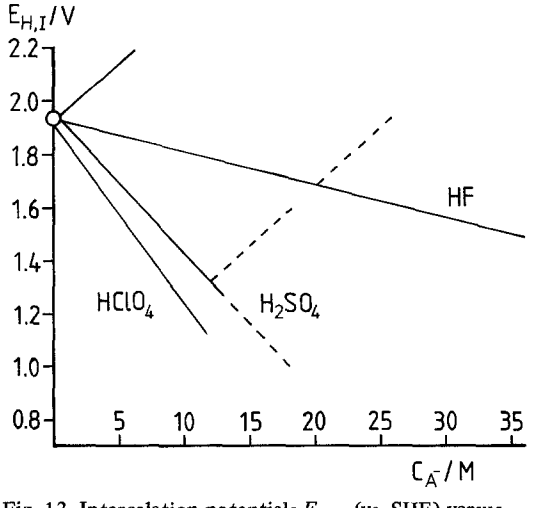

Fig. 13. Intercalation potentials $E_{H,I}$ (vs. SHE) versus molar concentration of anions. Descending curves: increasing acid concentration in solution. Ascending curves: increasing concentration of the intercalated anions. The potential grows by about 250 mV, if the surface concentration attains it's maximal value of 5.7 mol dm^{-3}.

4.4. *The intercalation potential*

Our results can only be understood, if a linear dependency of the intercalation potential on the surface concentration c_0 of the intercalated anion is assumed according to Equation 10. This is in parallel with the linear dependence of E_I on the acid concentration [6, 7, 9]. A common plot of all the results (Fig. 13) indicates, that there seems to be an absolute zero potential where neither an anion in the solution nor an anion in the solid is present ($E_{s,0} = 1.30$ V). The meaning of this point should be discussed further. It should be correlated with the graphite properties. The slope of the curve does not seem to depend strongly on the kind of intercalated anion. The dashed line indicates two cases, where the experiment is started from 12 mol dm^{-3} H_2SO_4 and from 20 mol dm^{-3} HF.

4.5. *Analysis of the rest potential time curves and corrosion*

After charging the CPP electrode, the rest potential decays more rapidly in the case of high charge than in the case of low charge. This is for two reasons. Generally, the concentration profiles of the intercalated anions tend to level out on standing. The rate increases with increasing initial surface concentrations. In addition to this, corrosion processes at the surface [7] increase with increasing c_0 in parallel, as clearly demonstrated by our

corrosion results in Table 1. An example of exhaustive corrosion is given in [6] Fig. 9. In many cases, a maximum concentration will be built up well below the surface of the electrode.

4.6. *Analysis of the discharge curve*

The S-type discharge curve indicates a stronger diffusion polarization, as expected compared with the charge curve. At the end of discharge, the surface concentration is nearly depleted, and the diffusion overpotential increases dramatically. In an experiment in 20 mol dm^{-3} HF, $t_{ch} = 30$ min, $j_{ch} = 3$ mA cm^{-2}, the high rate discharge with $j_{dis} = 30$ mA cm^2 down to $E_s = 0$ V yielded 85 mA min cm^{-2}, this means that $\alpha = 95\%$. A further discharge at 1 mA cm^{-2} gave an additional 2.9 mA min cm^{-2}, giving a total α value of 98%. In the opposite case, the results do not look so good, cf. example (1) in Fig. 8. As already mentioned, this is due to the formation of graphite oxide in the later stages of the high rate charging process.

5. Concluding remarks

Our results show clearly, that the CPP electrode is very useful as a positive electrode in secondary cells. Formation of the electrode is attained after a few cycles in a very simple manner. The potential is high and the reaction is reversible. Moreover, high current efficiencies are observed, even after several hours standing. After formation the CPP electrode seems to be in a practical form for use as a natural graphite bed electrode. The part at the electrolyte interface can be regarded as a well-contacted bed electrode. The part in the bulk remains unchanged and acts as a low cost feeder electrode.

The practical implications of the new electrode in secondary cells with Cu, Pb, Fe and Zn are under investigation [8]. As already mentioned in Section 1, high cycle numbers have been observed in some systems.

Acknowledgements

The authors acknowledge financial support of this work by MWF (Minister of Science and Research) of Nordrhein-Westfalen. We would like to express our gratitude to BASF Aktiengesellschaft, Ludwigshafen, especially to Dr Boehlke and Dr Theyson, for kindly providing the CPP material.

References

[1] W. Rüdorff and U. Hofmann, *Z. Anorg. Allg. Chem.* **238** (1938) 1.
[2] W. Rüdorff, *Adv. Inorg. Chem. Radiochem.* **1** (1959) 223. (cf. L. B. Ebert, *Ann. Rev. Mater. Sci.* **6** (1976) 181).
[3] A. R. Ubbelohde, M. J. Homley, G. S. Parry and D. A. Young, *J. Chem. Soc.* (1963) 5674.
[4] F. Beck, *Chem.-Ing.-Techn.* **46** (1974) 127.
[5] F. Beck, BMFT Final Report FB T 79-142 December 1979 "Entwicklung eines Bleitetrafluoborat Akkumulators".
[6] F. Beck, H. Krohn and H. Junge, *12th Int. Power Sources Symp.* Brighton, Sept. 1980. 'Power Sources', Vol. 8 (edited by J. Thompson) Academic Press, London (1981).
[7] F. Beck, H. Junge and H. Krohn, *Electrochim. Acta* **26** (1981) 799.
[8] F. Beck and H. Krohn, 'DECHEMA Monographien', Vol. 92 Verlag Chemie, Weinheim (1982).
[9] F. Beck, W. Kaiser and H. Krohn, *Angew. Chem. Suppl.* (1982) 57. *Angew Chem.* **94** (1982) 83.
[10] H. Krohn and F. Beck, *Ber. Bunsengesellschaft Physik. Chem.* (1982) forthcoming.
[11] F. Beck, R. Wurmb and K. Boehlke, German Patent Application 2 532 512 (1975 to BASF).
[12] F. Beck in 'The Electrochemistry of Lead' (edited by A. T. Kuhn), Academic Press, London (1979).
[13] H. P. Boehm, M. Eckel and W. Scholz, *Z. Anorg. Allg. Chem.* **353** (1967) 236.
[14] J. O. Besenhard and H. P. Fritz, *Z. Anorg. Allg. Chem.* **416** (1975) 106.
[15] H. S. Carslaw and J. C. Jaeger, 'Conduction of Heat in Solids,' Oxford University Press, Oxford (1947) p. 104.
[16] W. T. de Vries, *J. Electroanal. Chem.* **9** (1965) 448.
[17] S. Atlung, K. West and T. Jacobsen, *J. Electrochem. Soc.* **126** (1979) 1311.